

A SHOCK TUBE STUDY OF METHANE OXIDATION

Daniel J. Seery and Craig T. Bowman

United Aircraft Research Laboratories
East Hartford, Connecticut 06108

Although the oxidation of methane has been studied extensively there are still many unsolved problems related to the kinetics and mechanism of the reaction. The objective of the present investigation is to provide information on the reaction mechanism and chemiluminescence for the high temperature oxidation of methane. To this end an experimental study of methane oxidation behind reflected shock waves has been carried out. In this study pressure, OH, CH, CO, C₂ and H₂O emission and OH absorption were monitored during the reaction. In conjunction with the experimental work, an analytical study of methane oxidation was carried out. Using a proposed fifteen-step reaction mechanism, temperature, pressure and concentration profiles were calculated for the conditions of the experiment.

EXPERIMENTAL

The experimental study was carried out in a stainless steel cylindrical shock tube (shown in Fig. 1) having an internal diameter of 3.8 cm. The driver gas used in all experiments was room-temperature helium. To assure uniform diaphragm bursting pressures, a double diaphragm technique was employed (Ref. 1). Shock velocities were measured using four platinum heat transfer gauges mounted along the wall of the tube. The signals from these heat transfer gauges were displayed on a raster-sweep oscilloscope. The observation station was located 5.70 m from the diaphragm, and consisted of four observation ports. These ports were used to make various spectroscopic and pressure measurements. The reaction was studied behind reflected shock waves at a location 1 cm from the reflecting surface. This configuration gave a maximum test time of approximately 2 msec.

Pressure measurements were made using a piezoelectric pressure transducer (Kistler Model 605) with a 0.375 cm diameter pressure-sensitive diaphragm and a rise time of 3 μ sec. Two optical paths were available to monitor the emission and/or absorption of characteristic radiation during the reaction. The principal spectroscopic instrument was a 0.5 m Seya-Namioka vacuum monochromator equipped with an EMI/US 6255B photomultiplier. The entrance and exit slit widths were set to give a bandwidth of approximately 25 Å. The monochromator was used for both emission and absorption experiments. For the absorption experiments a Hg-Xe arc lamp (Hanovia 528B-1) was employed. Additional emission data were obtained from the other optical station using an EMI/US 9558BQ or a Philips 56CVP photomultiplier with various narrow-band pass interference filters. Sapphire windows were used for all optical stations. The output signals from the pressure transducers and photomultipliers were displayed on two dual-beam oscilloscopes which were triggered by one of the heat transfer gauges. The rise time of the photomultiplier/oscilloscope system was 2-3 μ sec.

The methane, oxygen and argon used in the experiments were Matheson Ultrapure Grade (>99.9%), and the nitrogen was Linde High Purity Dry (99.9%).

Gas mixtures were prepared manometrically and stored in stainless steel or glass vessels. These vessels were evacuated to a pressure of less than 1μ Hg before preparing the mixture. Mixture total pressures varied from 300-3000 mm Hg. Composition of the gas mixtures was confirmed using a mass spectrograph. The mixtures were allowed to stand for at least 48 hours before use in an experiment.

Before a run, the experimental section of the shock tube was evacuated to less than 1μ Hg. The leak and outgassing rate was less than 2μ Hg/min. Initial pressures of the gas in the experimental section varied between 15-150 mm Hg.

In all the experiments the temperature behind the reflected wave was obtained from the ideal shock equations and the measured incident shock velocity at the reflecting surface with a suitable correction for "non-ideal" shock reflection (Refs. 2 and 3). In the present investigation a temperature correction of -35 deg K with an uncertainty of 35 deg K was employed. This correction was based on the results of a study of reflected shock temperature in argon. In this study reflected shock temperatures were obtained from measurements of incident and reflected shock velocities using an approach suggested by Skinner (Ref. 3). This approach could not be used with the fuel/oxidizer mixtures due to gas dynamic acceleration of the reflected shock wave in the vicinity of the reflecting plate. Hence a direct determination of a temperature correction was not possible for the fuel/oxidizer mixtures.

Due to boundary layer effects, the pressure behind the reflected shock wave decreased in time. It was assumed that pressure and temperature behind the reflected wave were related through the isentropic equations. This assumption is not strictly correct due to heat transfer and chemical reaction effects. It is felt, however, that the error introduced by this assumption is small.

The temperature for a given run was assumed to be a linear average of the temperature directly behind the reflected shock wave (corrected for "non-ideal" reflection) and the temperature directly before the increase in pressure accompanying the chemical reaction. A similar averaging technique was employed for the pressure. Since variations in temperature and pressure behind the reflected wave were small, a linear averaging is acceptable.

EXPERIMENTAL RESULTS

The oxidation reaction was studied using pressure measurements and spectroscopic observations. The spectroscopic measurements involved the emission and absorption of the OH radical (3067 Å) and the emission of CH (4315 Å), CO (2200 Å), C₂ (5165 Å) and H₂O (9300 Å). Typical oscilloscope traces are shown in Figures 2, 3 and 4. The bottom trace in Figures 2 and 3 is the output of the pressure transducer. The arrival of the incident and reflected shock waves at the observation station and the increase in pressure due to chemical reaction are indicated in the figures. The top trace in Fig. 2 is the photomultiplier output showing OH emission. From the pressure and OH emission traces of Fig. 2 it is seen that the reaction appears to pass through two phases - a first (induction) phase in which the pressure and OH emission increase slowly followed by a second phase in which the pressure and OH emission increase rapidly. As will be discussed later, these observations are consistent with the results of the analytical study. The top trace in Fig. 3 is the photomultiplier output showing CH emission. From this figure it is seen that excited CH(²Δ) is probably short-lived, undergoing a maximum in concentration just prior to the onset of fast reaction. In Fig. 4 the top trace is the photomultiplier output showing OH emission and the bottom trace shows OH absorption. It is apparent that the onset of emission and absorption occur simultaneously, indicating that the concentration of excited state (²Σ) and ground state (²Π) OH increase approximately at the same time.

For the purpose of comparing the experimental and analytical results it is convenient to characterize the oxidation of methane by an induction time. There is no generally accepted definition of induction time. In the present study the induction time was defined to be the time between the heating of the gas by the reflected shock wave and the rapid increase in pressure or characteristic emission or absorption. This definition permits a simple comparison between experimental and analytical results and is not dependent on the threshold of the instrumentation.

Induction time data for methane oxidation are presented in Figs. 5 through 8. In these figures the mole percent of methane, oxygen and argon or nitrogen in the mixture is given together with the fraction stoichiometric, Φ , where

$$\Phi = \frac{(X_{\text{CH}_4}/X_{\text{O}_2})}{(X_{\text{CH}_4}/X_{\text{O}_2})_{\text{stoichiometric}}}$$

and X is the mole fraction. The solid lines through the data points are a least-squares fit of the experimental data to an equation of the form

$$\tau = A \exp (E/RT)$$

where τ = induction time, T = temperature, and A and E = constants. The parameters A and E and the standard deviation in E are obtained from the least-squares reduction of the data, and are tabulated in Table 1.

Table 1. Least-Squares Parameters: Methane-Oxygen-Diluent

Φ	Diluent	$P(\text{atm})$	$A(\text{sec})$	$E\left(\frac{\text{kcal}}{\text{mole}}\right)$	σE
0.5	N_2	1.7	1.6×10^{-10}	44.7	3.7
0.5	Ar	1.7	2.3×10^{-10}	44.3	1.4
0.5	Ar	3.7	4.5×10^{-11}	46.6	4.3
0.5	Ar	6.0	2.1×10^{-12}	53.2	6.0
1.0	Ar	2.0	5.8×10^{-11}	49.0	2.1
2.0	Ar	1.7	2.1×10^{-10}	45.4	4.8

The induction time for oxidizer-rich ($\Phi = 0.5$) methane/oxygen/argon and methane/oxygen/nitrogen mixtures for an average pressure of 1.7 ± 0.3 atm is presented as a function of temperature in Fig. 5. In this figure the induction time is based on the rapid increase in pressure. It is noted that in the present study there was no observed difference between induction times based on rapid increase in pressure or those based on rapid increase in characteristic emission or absorption. The solid line is the least-squares fit of the methane/oxygen/argon data. From Fig. 5 and Table 1 it is seen that within the experimental uncertainty and for a given temperature the induction time is the same for the methane/oxygen/argon and the methane/oxygen/nitrogen mixtures. Hence for the conditions of the present investigation replacing nitrogen by argon in the oxidizer does not have a significant effect on the induction time.

The induction time for a stoichiometric methane/oxygen/argon mixture at an average pressure of 2.0 ± 0.3 atm is presented as a function of temperature in Fig. 6. From this figure it is seen that there is no significant difference between induction times based on OH emission or OH absorption.

The dependence of the induction time on the fraction stoichiometric ($\Phi = 0.5, 1.0, 2.0$) is presented in Fig. 7. The difference between the least-squares lines shown in this figure are within the experimental uncertainty presented in Table 1. Therefore there is no significant variation of the induction time with fraction stoichiometric in the range of $\Phi = 0.5$ to 2.0 (for induction times between $50 \mu\text{sec}$ and 1 msec).

A comparison of the induction times for an oxidizer-rich methane/oxygen/argon mixture ($\Phi = 0.5$) at average pressures of 1.7 ± 0.3 atm, 3.7 ± 0.4 atm and 6.0 ± 0.3 atm is presented in Fig. 8. It is apparent that for a given temperature as the pressure increases from 1.7 atm to 3.7 atm the induction time decreases. As the pressure increases to 6.0 atm no further decrease in induction time is observed. Also shown on Fig. 8 is a least squares fit of the ignition delay data of Snyder, et al (Ref. 4) for CH_4 -air, $P = 4$ atm and $\Phi = 0.5$. It is seen that there is good agreement between the two sets of data.

ANALYTICAL INVESTIGATION

In order to gain insight into the reaction mechanism for methane oxidation and to aid in understanding the experimental results a model calculation was performed using a fifteen-step reaction mechanism. The calculations were made using a computer program which numerically integrates the system of reaction kinetic and state equations to give the time rate of change of compositions and thermodynamic properties. In the present study the calculations were made assuming an adiabatic, constant volume reaction. Hence the model calculation closely approximates conditions behind a reflected shock wave.

The mechanism for methane oxidation at high temperature is probably different from the low-temperature, low-pressure mechanism of Enikolopyan (Ref. 5) which is used by many investigators. It is more probable that the same reactions that are important for methane flame propagation also are important in the high temperature oxidation of methane. The reaction mechanism and rate constants used for the calculations are presented in Table 2.

Table 2. Reaction Mechanism

Reaction	Rate Constant = $A \exp(-B/T)$		Ref.
	A*	B	
1. $\text{CH}_4 \rightarrow \text{CH}_3 + \text{H}$	3.8×10^{14}	51,900	6
2. $\text{CH}_4 + \text{H} \rightarrow \text{CH}_3 + \text{H}_2$	2.0×10^{14}	5,800	7
3. $\text{CH}_4 + \text{OH} \rightarrow \text{CH}_3 + \text{H}_2\text{O}$	2.85×10^{13}	2,500	8
4. $\text{CH}_4 + \text{O} \rightarrow \text{CH}_3 + \text{OH}$	1.0×10^{13}	4,030	7
5. $\text{CH}_3 + \text{O}_2 \rightarrow \text{CH}_2\text{O} + \text{OH}$	1.0×10^{11}	-0-	9
6. $\text{CH}_3 + \text{O} \rightarrow \text{CH}_2\text{O} + \text{H}$	1.9×10^{13}	-0-	7
7. $\text{CH}_2\text{O} + \text{OH} \rightarrow \text{HCO} + \text{H}_2\text{O}$	3.5×10^{14}	503	9
8. $\text{HCO} + \text{OH} \rightarrow \text{CO} + \text{H}_2\text{O}$	$5.4 \times 10^{12} T^{0.5}$	252	9
9. $\text{CO} + \text{OH} \rightarrow \text{CO}_2 + \text{H}$	3.1×10^{11}	300	8

Table 2. Reaction Mechanism (Continued)

Reaction	Rate Constant = $A \exp(-B/T)$		Ref.
	A*	B	
10. $H + O_2 \rightarrow OH + O$	2.2×10^{14}	8,310	9
11. $O + H_2 \rightarrow OH + H$	1.1×10^{13}	4,730	9
12. $O + H_2O \rightarrow 2OH$	4.2×10^{13}	9,120	9
13. $H + H_2O \rightarrow H_2 + OH$	5.0×10^{13}	10,100	9
14. $H + H + M \rightarrow H_2 + M$	$5.0 \times 10^{18} T^{-1}$	-0-	9
15. $H + OH + M \rightarrow H_2O + M$	$4.5 \times 10^{21} T^{-1}$	-0-	9

* A is in $\text{cm}^3 \text{mole}^{-1} \text{sec}^{-1}$ except for (1) where the units are sec^{-1}

This mechanism is derived primarily from the flame studies of Fristrom and Westenberg (Ref. 7) and Fenimore and Jones (Ref. 9) plus the methane dissociation reaction to assist the initiation.

DISCUSSION

Before proceeding to a discussion of the experimental data it is of interest to consider some of the results of the analytical study (Figs. 9 and 10). Figure 9 shows the calculated temperature and pressure profiles for an initial temperature of 2000 deg K, an initial pressure of 3.4 atm and 0.5 fraction stoichiometric. The temperature and pressure increase slowly during the induction period and then increase rapidly. Calculated concentration profiles for several important species for the above conditions are presented in Fig. 10. The concentrations of the intermediates increase very rapidly during the early stages of the reaction and then maintain a nearly constant value through most of the induction period. The product species have different concentration profiles. CO and H₂O show a rapid increase early in the induction period and then increase almost linearly to their equilibrium concentrations. CO₂, on the other hand, increases almost linearly from the start and only at the very end of the induction period does it increase rapidly.

Calculations similar to those discussed above also have been made for initial temperatures of 1900 deg K and 1800 deg K (stoichiometry and initial pressure were identical with the 2000 deg K calculation). Qualitatively the temperature, pressure and concentration profiles are the same as for the 2000 deg K calculation except on a longer time scale. Since the calculated and observed pressure profiles are qualitatively the same, it is possible to compare calculated and observed induction times (based on rapid increase in pressure). The calculated induction times, presented in Fig. 8, exceed the experimental values by a factor of ten at 1800 deg K and by a factor of five at 2000 deg K. Considering the uncertainty in some of the

specific rate constants used in the reaction mechanism the difference between experiment and analysis is not unexpected. As an example, if the rate constant for reaction 10 is varied by a factor of ten there is a 30-40 percent variation in the calculated induction time at 2000 deg K. At lower temperatures variations in the rate constants of chain-branching reactions could have an even greater effect on the calculated induction times. In addition the neglect of certain chemical species in the analysis (e.g. HO_2 and H_2O_2) may contribute to the discrepancy especially at the lower temperatures.

At the present time the calculated concentration profiles only can be compared qualitatively with the experimental data. In particular it is noted that after the first few microseconds the calculated OH concentration increases approximately exponentially in time. Experimental results indicate that OH absorption (which is a measure of ground state OH concentration) also increases approximately exponentially in time.

It is of interest to compare the time variation of CH and OH emission and OH absorption in methane oxidation with similar observations in acetylene oxidation. Stubbeman and Gardiner (Ref. 10) have studied the oxidation of acetylene in a shock tube and observed OH emission and absorption (3067 Å) and visible chemiluminescence (4320 Å). It is probable that the 4320 Å emission is due to the ${}^2\Delta$ - ${}^2\Pi$ transition in CH. During the reaction a peaking of the 4320 Å emission (similar to that shown in Fig. 3) was observed. Coincident with the 4320 Å peak a pulse of OH emission at 3067 Å was observed. Following the tail-off of emission an increase in OH absorption was observed. In methane oxidation a peaking of CH emission is observed (Fig. 3); however OH emission and OH absorption are found to increase simultaneously during the reaction. If the lag between CH emission and OH absorption in acetylene oxidation is real then there must be different mechanisms for chemiluminescence in methane and acetylene oxidation. Indeed, Deckers (Ref. 11) has suggested that in acetylene oxidation there are two possible reactions for producing CH (${}^2\Delta$) but that only one of the reactions is important in methane oxidation.

ACKNOWLEDGEMENTS

The authors thank T. F. Zupnik, Pratt & Whitney Aircraft, for providing the computer program used for the reaction kinetic calculations. This work was sponsored, in part, by the Air Force Aero Propulsion Laboratory (Wright-Patterson) under Contract No. AF 33(615)-3179.

References

1. Wurster, W. H., *J. Chem. Phys.*, 36, 2112 (1962).
2. Strehlow, R. A. and C. T. Case, *J. Chem. Phys.*, 35, 1506 (1961)
Johnson, C. D. and D. Britton, *J. Chem. Phys.*, 38, 1455 (1963).
3. Skinner, G. B., *J. Chem. Phys.*, 31, 268 (1959).
4. Snyder, A. D., J. Robertson, D. L. Zanders and G. B. Skinner, Shock Tube Studies of Fuel-Air Ignition Characteristics, Monsanto Research Corporation Report AFAPL-TR-65-93. August 1965.
5. Enikolopyan, N. S., Seventh Symposium (International) on Combustion, London, Butterworths (1959), p. 157.
6. Palmer, H. B. and T. J. Hirt, *J. Phys. Chem.*, 67, 709 (1963).
7. Fenimore, C. P. and G. W. Jones, *J. Phys. Chem.*, 65, 1532 (1961), *ibid.*, p. 2200.
8. Wilson, W. E., paper presented at 1967 Spring Meeting, Western States Section The Combustion Institute, LaJolla, Calif., April 24-25, 1967.
9. Fristrom, R. M. and A. A. Westenberg, Flame Structure, New York, McGraw-Hill, 1965. See also Fristrom, R. M., Ninth Symposium (International) on Combustion, New York, Academic Press (1963), p. 560.
10. Stubbeman, R. F. and W. C. Gardiner, Jr., *J. Phys. Chem.* 68, 3169 (1964).
11. Deckers, J. M., Energy Distribution in Flames and Electric Discharges, Final Report Grant AF-AFOSR 375-65, Lash Miller Chemical Laboratories, University of Toronto, August 1966.

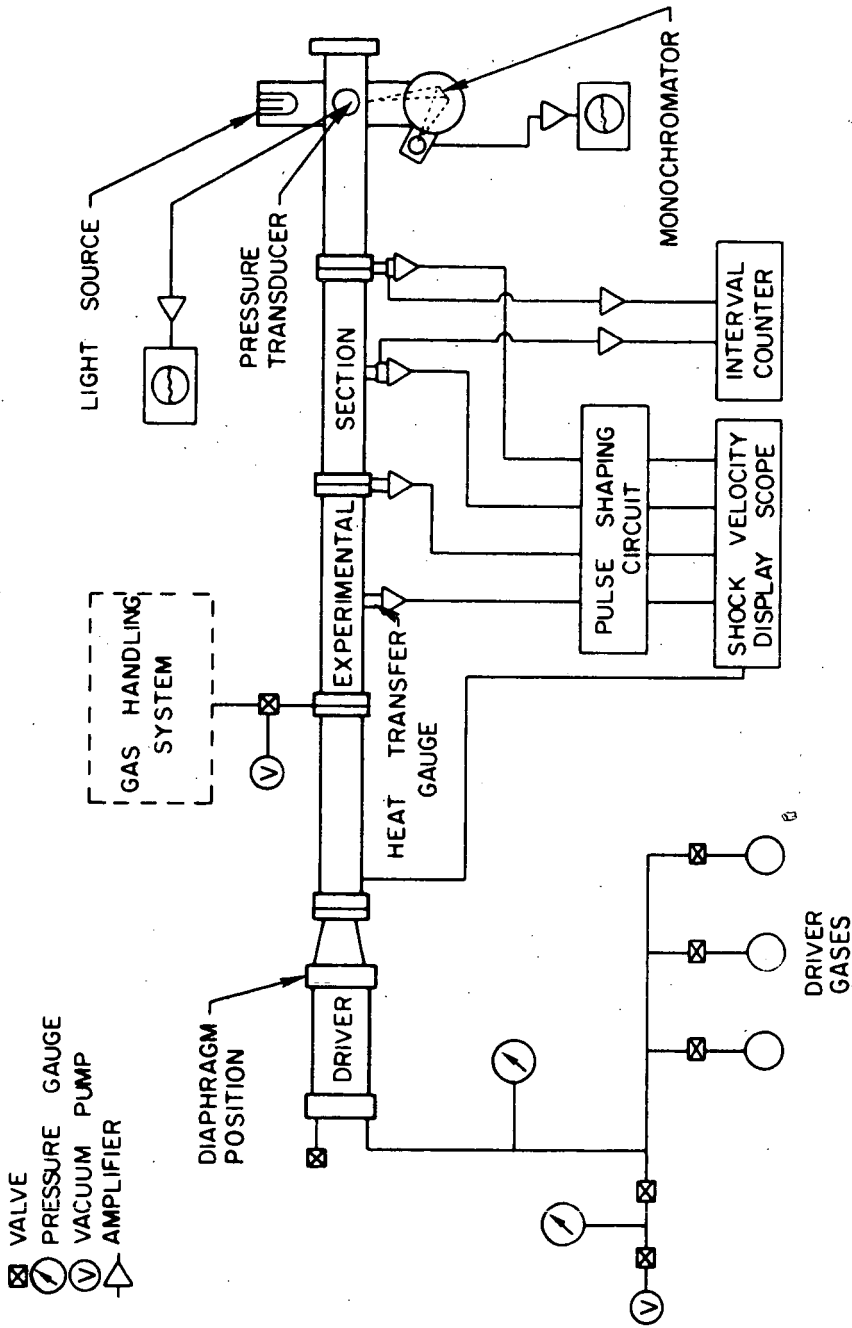


FIGURE 1. SCHEMATIC DIAGRAM OF EXPERIMENTAL APPARATUS

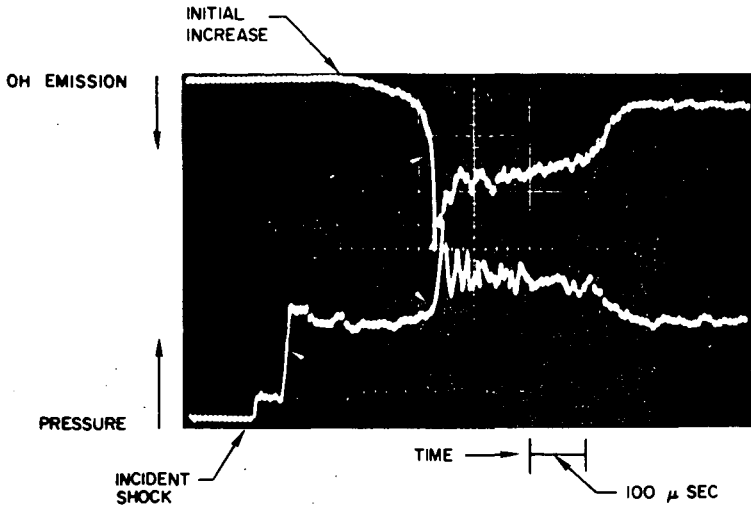


FIGURE 2. PRESSURE CHANGE AND OH EMISSION DURING INDUCTION PERIOD FOR METHANE IGNITION

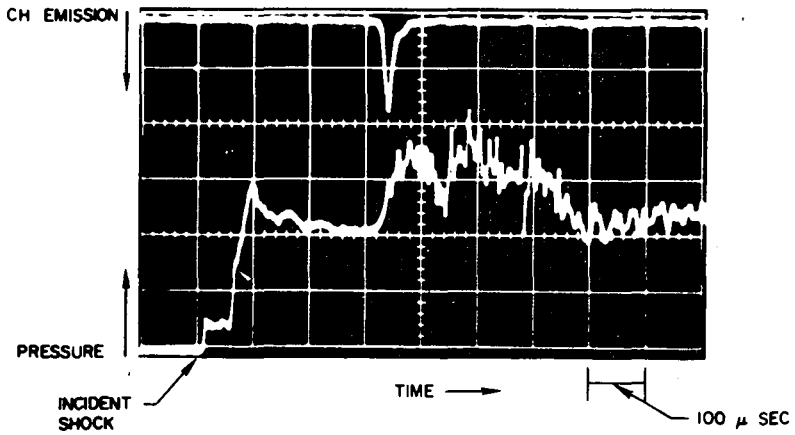


FIGURE 3. PRESSURE CHANGE AND CH EMISSION DURING INDUCTION PERIOD FOR METHANE IGNITION

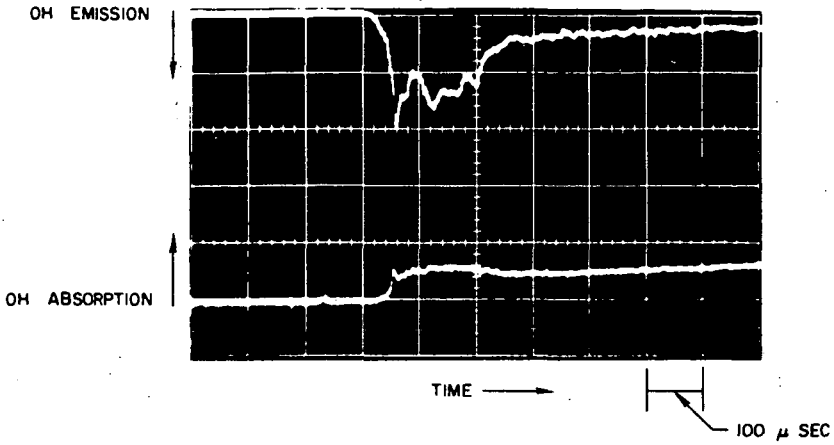


FIGURE 4. OH EMISSION AND ABSORPTION DURING INDUCTION PERIOD FOR METHANE IGNITION

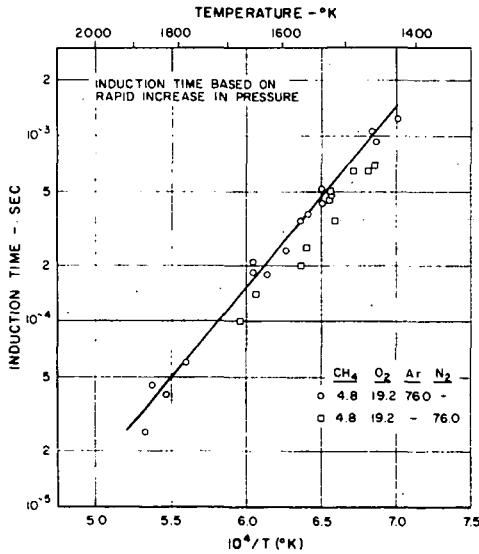


FIGURE 5. TEMPERATURE DEPENDENCE OF INDUCTION TIME FOR P=1.7 ATM AND $\phi = 0.5$

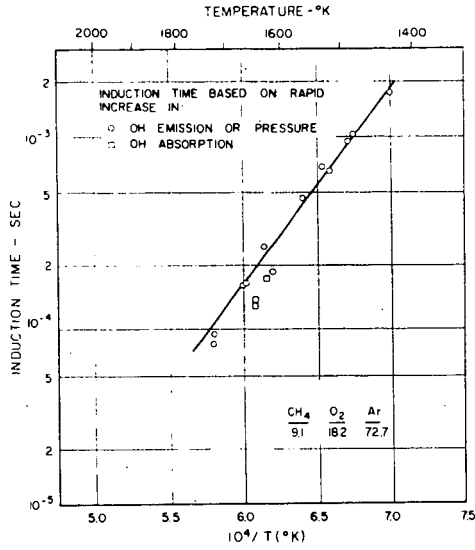


FIGURE 6. TEMPERATURE DEPENDENCE OF INDUCTION TIME FOR P = 2.0 ATM AND $\phi = 1.0$

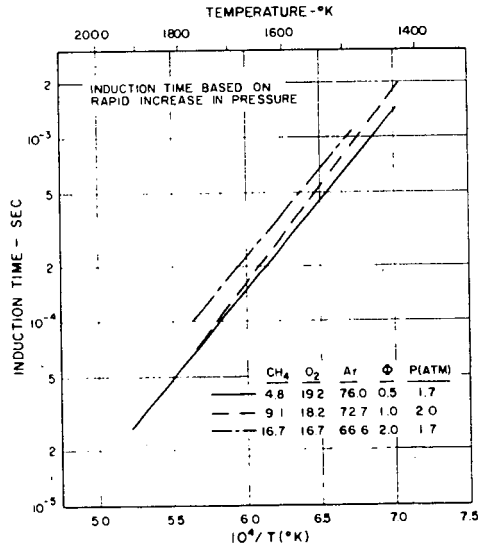


FIGURE 7. TEMPERATURE DEPENDENCE OF INDUCTION TIME FOR SEVERAL ϕ

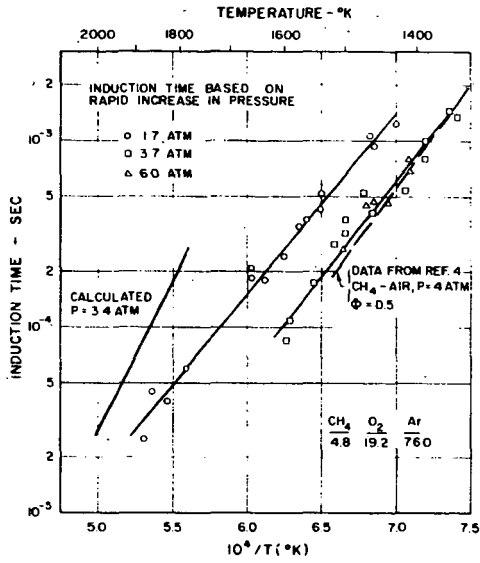


FIGURE 8. TEMPERATURE DEPENDENCE OF INDUCTION TIME FOR SEVERAL PRESSURES

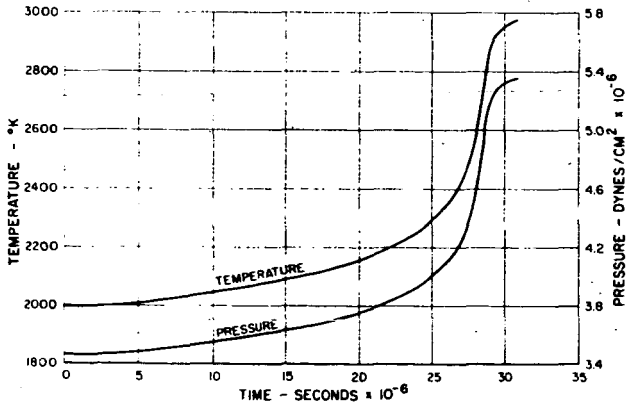


FIGURE 9. CALCULATED TEMPERATURE AND PRESSURE PROFILES FOR T = 2000°K, P = 3.4 ATM AND Φ = 0.5

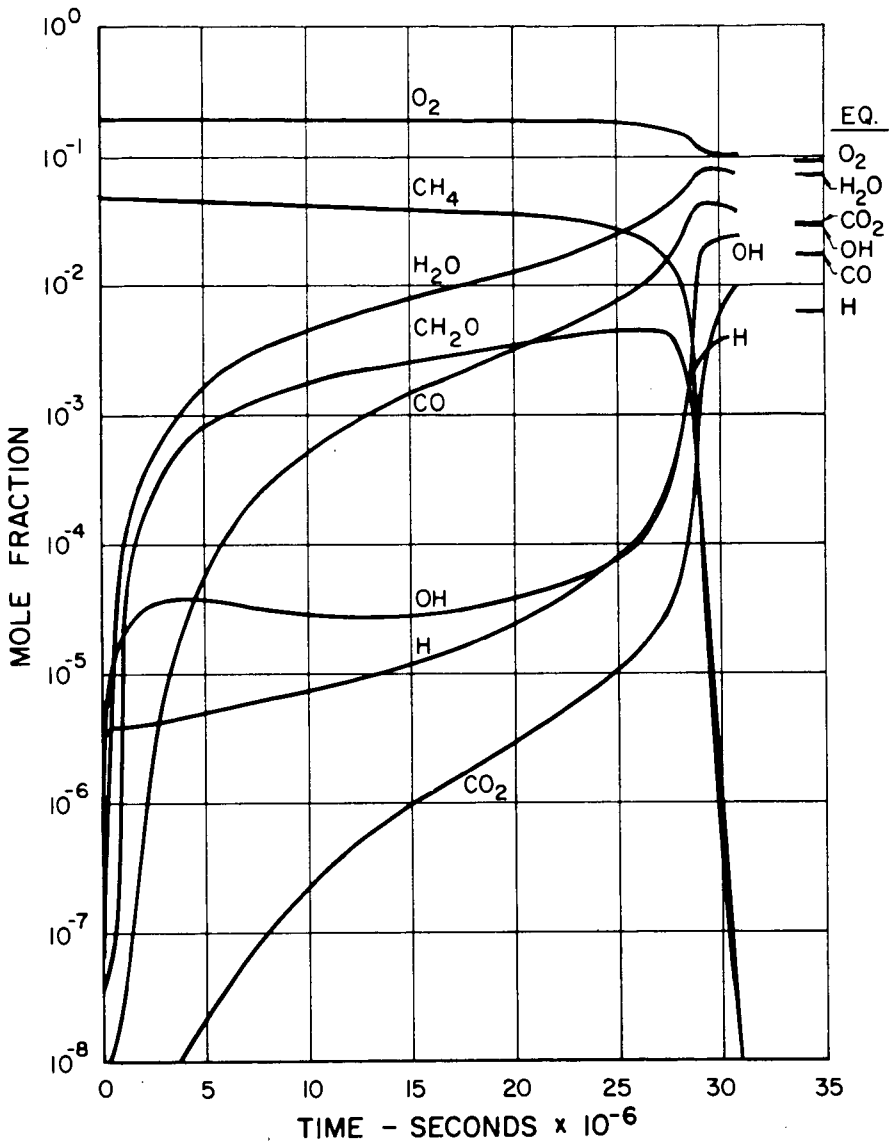


FIGURE 10. CALCULATED CONCENTRATION PROFILES FOR
 $T = 2000^\circ K$, $P = 3.4$ ATM AND $\Phi = 0.5$